Damping, Drive and Non-linear Effects of Kinetic Low-frequency Modes in Tokamaks

Ph. Lauber[1], M. Brüdgam[1], D. Curran[2], M. Sempf[1], V. Igochine[1], S. Günter[1], M. Maraschek[1], P. McCarthy[2], M. García-Muñoz[1] and the ASDEX Upgrade Team

[1]Max-Planck-Institut für Plasmaphysik, EURATOM-Association, D-85748 Garching, Germany
email: philipp.lauber@ipp.mpg.de
[2]Department of Physics, University College Cork, EURATOM-Association DCU, Cork, Ireland

1. Introduction

On the way to a comprehensive understanding of the properties of a burning plasma the physics of super-thermal particles due to external heating and fusion reactions plays a key role. Especially Alfvén and Alfvén-acoustic type instabilities are predicted to strongly interact with the fast particle population and to contribute critically to the radial redistribution of the energetic ions [1, 2, 3].
In this paper the role of low-frequency modes in the frequency range $\omega_A > \omega \simeq \omega_{ti} \gtrsim \omega_{bi} \gtrsim \omega_{p*}$ for the stability and the fast particle transport is investigated. Here, ω_A is the Alfvén frequency, ω_{ti} and ω_{bi} are the transit resp. bounce frequency of the thermal ions and ω_{p*} is the diamagnetic frequency. For typical ASDEX Upgrade parameters and low toroidal mode numbers $n = 2-6$, these frequencies are of the order $30-100$ KHz. It was reported that whenever modes in this frequency band are present, the direct (caused by the mode itself) and indirect (caused by other modes such as TAEs that are simultaneously present) fast particle losses increase significantly [4] . Therefore, these modes are not only effective in redistributing energetic particles in the plasma core ($\rho_{pol} = 0.1-0.4$) but also drive other modes more unstable that are localised further outside (for TAEs typically $\rho_{pol} = 0.6$) and that may have very different frequencies.
In the first part the linear properties of these modes are investigated using analytical theory and the linear gyrokinetic code LIGKA [5]. Especially the dependence on the background gradients and the inclusion of trapped particle dynamics is addressed. In the second part, the non-linear evolution of these modes and their interaction with TAE modes is investigated.

2. Local Analysis

The kinetic dispersion relation for this low frequency regime has been first derived in the ballooning representation [6] . A generalised expression including finite Larmor orbit and finite orbit width effects can be found in reference [7]. Several alternative derivations were reported recently [8, 9]. Elongation effects for the GAM dispersion relation that in the long wave-length limit is described by the same dispersion relation [10, 11, 12, 8, 13] were analytically and numerically investigated [14, 15]. Also trapped particles were included in the dispersion relation, demonstrating that the continuum accumulation shifts down in frequency with increasing trapped particle fraction [16, 17] . Furthermore, the importance of the sideband generation due to the asymmetry in the ω_* terms for mid-n MHD modes has been pointed out in [18, 17]
This dispersion relation predicts a splitting of the continuum minimum at the $q = 1$ surface for different poloidal and toroidal mode numbers ($n = m$). This splitting of the BAEs has been observed at Tore Supra[19], however no detailed mode number analysis was possible so far. The recent upgrades of the soft X-ray camera system at ASDEX Upgrade [20] motivated dedicated experiments concerning this issue. In fig. 1 the spectrograms of two central SXR channels

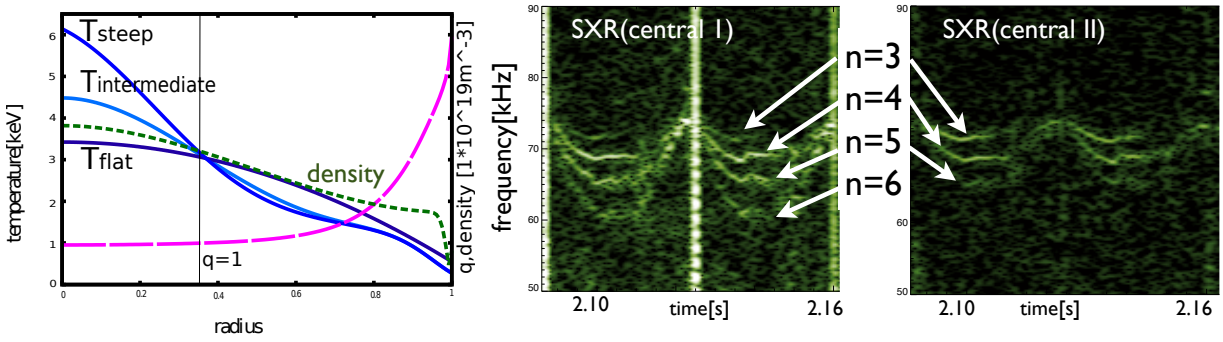

FIG. 1. Profiles for a model equilibrium based on the discharges #20488 and #25549 (left). Right: spectrogram of two central channels of the SXR camera show a splitting of the BAE mode (#25549). The correlation of several channels allows for a reliable determination of the poloidal mode numbers.

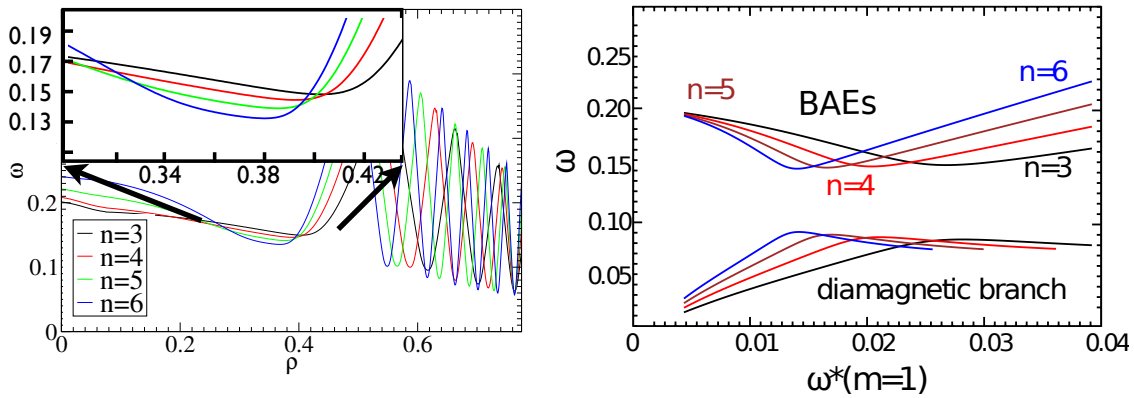

FIG. 2. The continuous spectrum for different toroidal/poloidal mode numbers shows a splitting of the accumulation point close to the $q = 1$ surface at $\rho_{pol} = 0.37$ (left); On the right, the influence of the background temperature profile on the BAE and the diamagnetic (BAAE) branch at the $q = 1$ surface is demonstrated. ω is normalised to the on-axis Alfvén frequency ω_A.

for discharge #25549 are shown. Two sawtooth periods with a crashes at $t = 2.08, 2.12$ and $2.16s$ are visible. Clearly, several modes in the BAE frequency regime can be seen. Different channels detect a different amplitude ratio of the individual modes (see middle and right spectrogram of fig. 1; in total 12 channels are available within the $q = 1$ surface) and in combination with a toroidal mode number analysis using the Mirnov coil system, the mode numbers $n = m = 3, 4, 5, 6$ could be determined with high confidence.

In order to model this splitting and its evolution during the sawtooth periods, the kinetic dispersion relation in the circulating particle limit was solved with a post-processing tool for the equilibrium code CLISTE [21, 22]. Figure 2 demonstrates that the accumulation point of the kinetic continuum at the $q = 1$ surface is not degenerated for different toroidal mode numbers (left) and for different values of the background gradients, $\omega_{p*} = \omega_{*n} + \omega_{*T} = T_i/(eB)k_\theta(\nabla n/n)(1+\eta)$ with $\eta = \frac{\nabla T}{T}/\frac{\nabla n}{n}$. A detailed analysis and comparison with the experiment, including q-profile, temperature and pressure variation for various discharges can be found in ref. [22]. As mentioned above, circulating particles with $v_\parallel/v < 1$ and trapped particles modify the continuous spectrum with respect to the $v_\parallel/v = 1$ case. For the three different temperature profiles of figure 1, figure 3 shows that there is not only a significant frequency downshift by about 20-30 % but also a shift into the stable part of the complex plane. Clearly this is due to an increasing ion Landau damping for lower frequencies. Nevertheless, in the case of the steep background

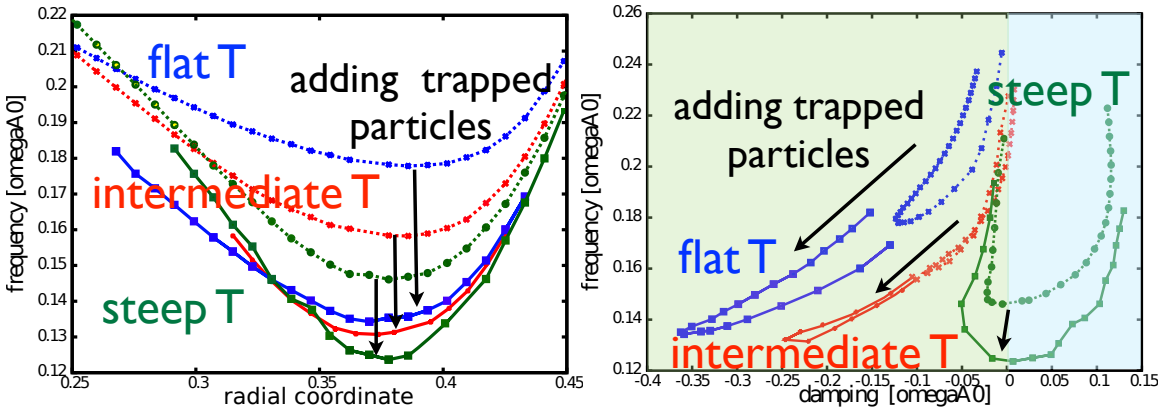

FIG. 3. The continuous spectrum for the profiles given in fig 1: the inclusion of trapped particles shifts down the real frequency close to the $q = 1$ surface at $\rho_{pol} = 0.37$ (left); the downshift increases ion Landau damping for flat temperature profiles (right). $\omega_{A0} = v_{a0}/R$ is $3.5 \cdot 10^6 rad/s$ for this example. The ratio of the thermal velocity to the Alfvén velocity, $v_{th}/(v_{A0})$ at the $q = 1$ surface is 0.09.

temperature gradient , the minimum of the continuum is marginally stable. This suggests that especially for higher mode numbers (in this example $n = 4$ was used) a destabilisation without energetic particles is possible [7], as will be demonstrated below.
Finally, it should be noted that only if the trapped particle dynamics is included, a good agreement ($\sim 5\%$) between the experimental frequencies and the accumulation point of the continuous spectrum can be found [22].

3. Global Analysis

So far it was assumed that the BAE modes are close to the accumulation point of the spectrum. This analytical prediction is tested by solving the full system of quasi-neutrality, gyrokinetic moment and gyrokinetic equation employing the linear eigenvalue code LIGKA. A new iterative method for finding the eigenvalues of a matrix whose elements depend in a non-linear way on the eigenvalues was tested and successfully compared to the Nyquist contour solver and the antenna version of the code. The combination of all the three methods allow for a fast and reliable detection of in principle all eigenmodes in the complex frequency plane. Also sub-dominant and heavily damped branches can be found and traced. In fig. 4 the electrostatic potential of the least damped eigenmodes, their mode frequency and their damping rates for the three different temperature profiles (fig. 1) are shown. As expected by theoretical analysis [8, 10], the modes are peaked around the $q = 1$ surface. Their radial width increases slightly with increasing temperature gradient. The mode frequency is close to the continuum accumulation point: for the flat and the intermediate profile it is slightly below, and for the steep profile it is above the accumulation point. In analogy to the TAE nomenclature, a mode above the continuum that couples to the kinetic Alfvén branch is called kinetic BAE (kBAE) [25] in the following. The red dashed line in fig. 4 demonstrates that the rather strongly damped mode - mostly by ion Landau damping - in the flat profile case ($\gamma/\omega = -7.0\%$) is destabilised by a steep background temperature profile ($\gamma/\omega = +1.0\%$). Other eigenmodes for T_{steep} with damping rates between -5 and -20% are shown in fig 5. With a slightly higher frequency than the continuum ($\omega = 0.127\omega_A; \gamma/\omega = -12\%$), a kBAE with a higher radial mode number (black dotted in fig. 5) than the most unstable kBAE in fig 4 was found. Below the continuum a mode exists that

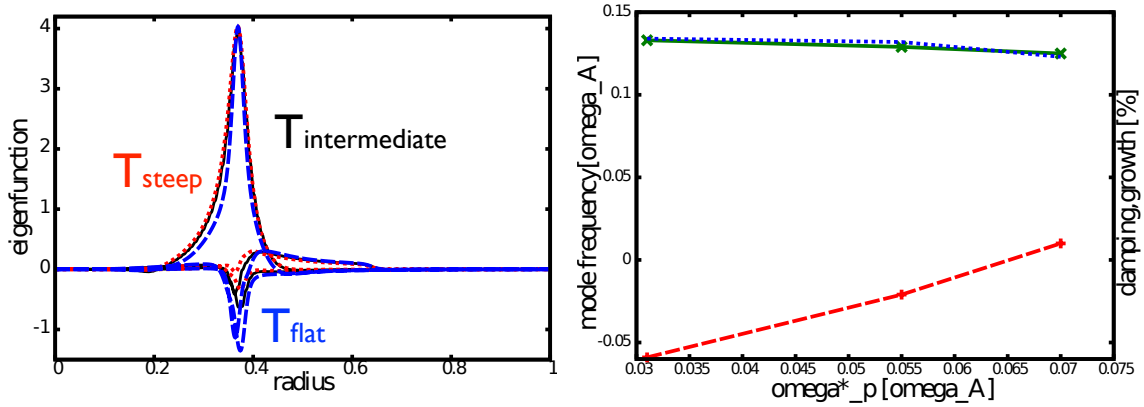

FIG. 4. Eigenfunctions of the least damped $n = 4$ BAE (electrostatic potential) for the three different temperature profiles of fig. 1; dashed: T_{flat}, solid: $T_{intermediate}$, dotted: T_{steep}. Right: corresponding BAE mode frequencies: the solid green line represents the real mode frequency, the dashed red line the damping resp. growth (in %!) and the dotted blue line shows the accumulation point of the continuum.

is strongly coupled to an acoustic mode at $\rho_{pol} = 0.2$. Whereas all the modes discussed before have a clear electromagnetic ('Alfvénic') polarisation, this mode has a strong electrostatic component (fig. 5, right) and is therefore strongly damped ($\omega = 0.120\omega_A; \gamma/\omega = -30\%$). At much lower frequency $\omega = 0.07\omega_A$ a mode with broader radial structure, different side band coupling, stronger electrostatic properties and moderate damping $\gamma/\omega = -7\%$ was found. This frequency regime corresponds to the BAAE range [23] in a fluid model. It should be noted that in this low frequency range fluid theory has only very limited validity and therefore mode frequency, mode structure and existence conditions can be very different in a MHD model compared to the results presented here. For a detailed discussion of the differences of kinetic and fluid theory see ref. [26].
Experimentally, both BAE and 'BAAE' can be driven unstable by energetic ICRF-generated ions. (It should be noted that the steep background temperature profile used here for demonstration purposes is exceeding typical experimental values, whereas the intermediate one is realistic.) It can be shown that for an isotropic slowing down distribution function the contribution of the real and imaginary part of δW_{fast} is such that it destabilises the mode and deepens the potential well for the localisation of the gap mode. For realistic, non-isotropic distribution functions also the energetic particle branches of the modes may be excited. Further analysis is on the way.

4. Non-linear consequences

The importance of these core localised modes becomes obvious when the overall transport of energetic particles is investigated. It is well known that several modes with similar frequency at different radial locations cause an increased transport due to resonance overlapping in phase space. Here the question is addressed, how modes with very different frequencies and resonance conditions $\omega - n\omega_{prec} - p\omega_b = 0$ can interact, e.g. TAEs and BAEs, as seen experimentally [4]. Here, ω is the mode frequency, ω_{prec} the toroidal precession frequency, n the toroidal mode number, ω_b the bounce frequency of the trapped particles and p numbers the bounce harmonics. Employing the drift-kinetic, non-linear HAGIS code[28] allows to identify not only the resonance conditions and the regions of overlap in phase space but also the overall mode saturation levels for single and multi-mode cases. Based on the ASDEX-Upgrade discharge #21083 (for the equilibrium parameters see ref. [4]) non-linear simulations were carried out

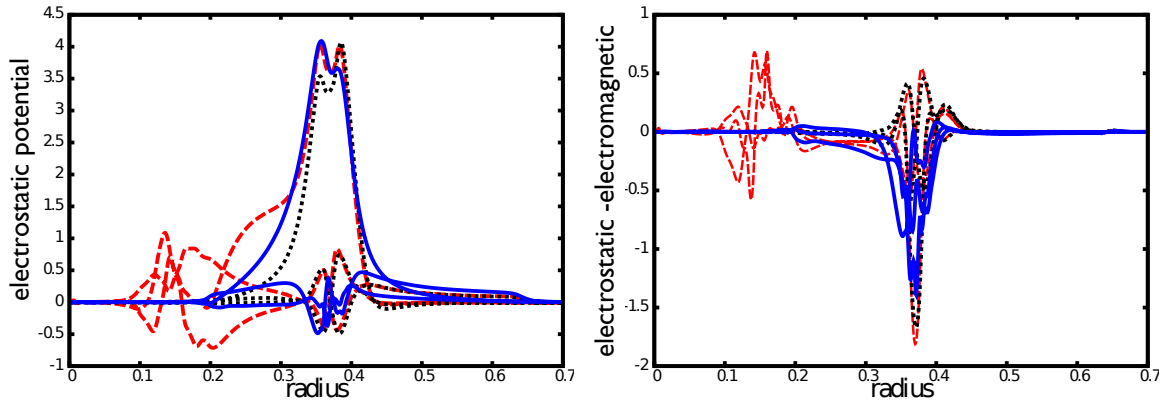

FIG. 5. Other eigenfunctions (electrostatic potential on the left and the difference between electrostatic and electromagnetic potential $\sim E$ on the right) for T_{steep} found with LIGKA*: one mode frequency is above the gap (kBAE, black dotted) and above the most unstable mode shown in fig. 4 , one below the gap (red dashed) and one in the very low frequency 'BAAE' regime (blue solid).*

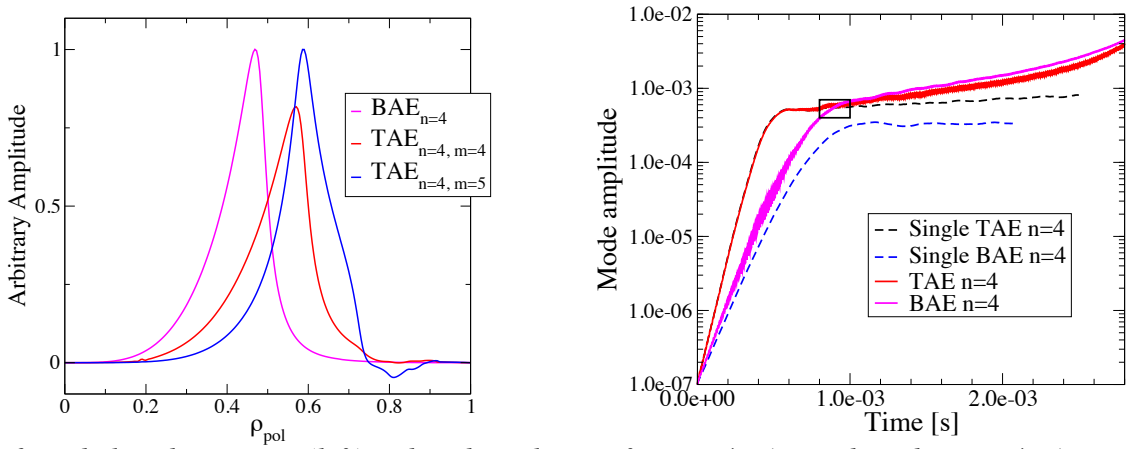

FIG. 6. Radial mode structure (left) and mode evolution of an $n = 4$ BAE mode and an $n = 4$ TAE mode (right): the dashed lines indicate runs where just one mode was present in the system, the solid lines show the evolution when both modes are present simultaneously.

with a fast particle distribution (hydrogen, fast deuterium neglected) that is is slowing down in energy and isotropic in pitch angle. Although this simplification is not true for ICRF generated energetic particles, it will allow one to first understand the qualitative features of the driving mechanism. Figure 6 shows the mode evolution of a single $n = 4$ BAE mode with $f_{BAE} = 50$kHz and a single $n = 4$ TAE mode with $f_{TAE} = 150$ kHz together with a case where both modes were simultaneously present. The drive $\beta_f = 0.3\%$ was kept constant. As expected for the single mode cases, the mode amplitude saturates once the fast particle gradient around at the position of the mode has flattened. In the case with both modes present , the TAE amplitude and growth rate is up to about $t = 1 \cdot 10^{-3}$s very similar to the single mode case, whereas the BAE growth rate is larger during the whole simulation time. Furthermore, when the BAE amplitude becomes comparable to the TAE amplitude at $t \approx 1 \cdot 10^{-3}$s, both mode start growing again to very high amplitudes.

This clearly demonstrates that there is an effective coupling mechanism between both modes. An analysis of the changes in phase space explains the mechanism: on the left of fig. 7 the resonance plot of trapped energetic ions in the energy-Z plane is shown. Here the coordinate

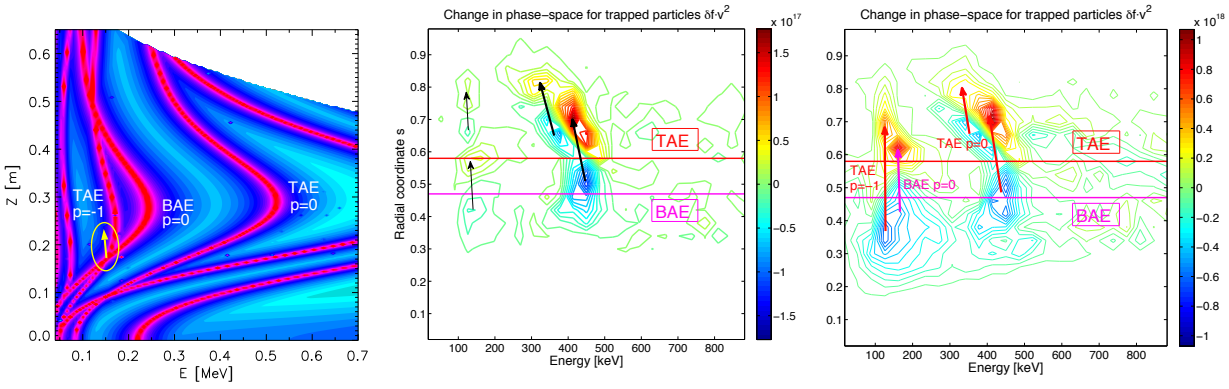

FIG. 7. A comparison of the resonance plot and the actual distribution of fast particle density (pressure) for early and late times of a non-linear simulation with both BAE and TAE present. The horizontal lines indicate the peaks of the radial mode structure. Note that the plot on the left is valid for on-axis energetic particles ($\lambda = 0$), whereas the other graphs represent a pitch angle averaged pressure.

Z represents the vertical distance in meters from the magnetic axis to the turning point of the trapped particles. The colored lines represent the resonance conditions $\omega - n\omega_{prec} - p\omega_t = 0$ for both modes ($n = 4$) and various bounce harmonics p. The middle graph of fig. 7 shows the change of phase space density weighted with the velocity square v^2 of the redistributed energetic particles at an early time in the simulation ($t = 4.0 \cdot 10^{-4}$), representing the energy transfer between particles and the wave. One can see that the TAE is predominantly driven by the $p = 0$ resonance at an energy of $E \approx 400 - 500$ keV at this early stage. Trapped particles with higher energies and circulating particles are not contributing significantly to the mode drive. The redistribution pattern (blue regions represent a decrease of fast particle pressure, red regions an increase) lines up very well with the resonance plot on the left. Note that the Z-axis and the normalised minor radius are approximately equivalent in these plots. Since there is no BAE resonance close to this main TAE ($p = 0$) resonance in phase space, no additional BAE drive due to the TAE is expected in this part of the phase space. However, there is an overlap of the two resonances, $p = -1$ for the TAE and $p = 0$ for the BAE, at around $E = 150$keV. By comparing this low frequency redistribution to the single TAE case (not shown here) and recalling that the BAE amplitude is very small at this early time one can conclude that the redistribution is caused almost only by the TAE. As the amplitude of the TAE increases (driven mainly by $p = 0$ resonance), also the redistribution at the $p = -1$ resonance becomes more effective due to the higher mode amplitude. As a consequence, the energetic particle gradient at the BAE position increases due to the TAE. This explains the extra drive of the BAE due to the TAE compared to the single BAE case. At $t = 6.0 \cdot 10^{-4}$ the TAE saturates, while the BAE is still growing since it taps a different energy reservoir in phase space than the TAE. Once the BAE amplitude reaches the same amplitude as the TAE , it provides an extra drive for the TAE, as can be seen in the graph on the right in fig. 7: close to the overlapping region both modes redistribute particles efficiently and the BAE increases the energetic particle gradient at the position of the TAE. At this point, both modes can tap a larger reservoir of energy in phase space than the single modes and therefore a further growth of both modes is observed.

The particles that are in resonance with both modes of the same toroidal mode number play a special role. If their bounce frequency is equal to the difference frequency $\Delta\omega = \omega_{TAE} - \omega_{BAE}$, the particles stay in resonance with both modes and therefore couple their amplitudes: since they are radially 'trapped' between both modes, they transfer energy from the mode with higher amplitude to the mode with lower amplitude [27] .

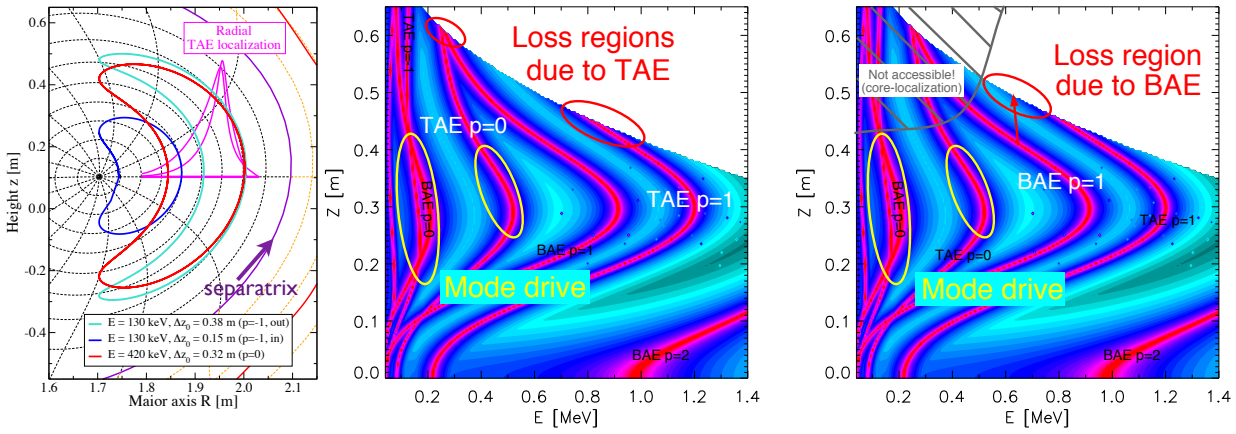

FIG. 8. typical orbits for particles from the region in phase space where the energy exchange is maximal (left). Middle and right: resonance plots summarising mode drive and loss regions for TAE and BAE.

5. Particle Losses

In this section the energetic particle losses due to the wave-particle resonances are analysed. Looking at the particle orbits corresponding to the resonant regions in phase space reveals that there is a difference between particles that dominate the drive and particles that are expelled from the plasma region and hit the first wall and the fast ion loss detector. Although fig. 7 shows an increased density relatively close to the loss boundary, fig. 8 (left) demonstrates that the particle orbits at the critical resonance areas are not wide enough (even if their gyro-radius is included) to directly leave the plasma (see e.g. the 420keV particle in fig. 8). However, particles at higher energies with larger drift orbits, or particles localised further outside can be expelled easily because their resonance branches directly intersect the loss region. A small radial displacement due to the resonant wave field is sufficient to move them on a loss orbit.

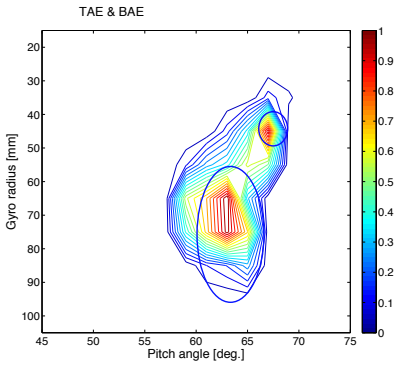

FIG. 9. Loss pattern (normalised to the maximal loss amplitude) at the detector position including finite Larmor-radius effects, calculated with the extended HAGIS *code. The ellipses indicate the experimental result [4], taking into account drift corrections in the detector.*

These regions are the ones indicated by the red ellipses in fig. 8. Note that due to the core localisation of the BAE there are no low-energy losses although there are intersections of the resonance branches and the loss region. Employing the extended version of HAGIS with a vacuum region and a detailed model for the fast particle detector [27], allows to map the losses on a pitch angle - energy plane and thus directly compare to the data obtained with the fast ion loss detector at ASDEX Upgrade [29]. Fig. 9 shows the loss pattern in direct comparison to the experimental measurements [4]. For this plot, only trapped particles were considered that have their turning point close to the magnetic axis. Remarkable agreement is found, validating the code extension and the numerical model for the detector. Inaccurate modelling assumptions such as a more localised BAE eigenfunction as observed in the experiment and a more realistic ICRF distribution function are

expected to change some quantitative features of these results (absolute amplitudes) but not the qualitative picture of the loss mechanism, as discussed in ref. [27].

6. Conclusions and Outlook

In this paper the properties of low-frequency Alfvén-Acoustic modes are discussed and their influence on energetic particle transport are investigated: in order to quantitatively analyse the shear-Alfvén-acoustic continuum at and below ω_{BAE} and compare to the experiment, a kinetic dispersion relation including diamagnetic effects is required. Also trapped particle dynamics becomes increasingly important as the mode frequencies decrease. Several stable eigenmodes were found numerically close to the BAE accumulation point. Their existence depends inter alia on the background gradients and they can be driven unstable - despite strong ion Landau damping - by steep enough background temperature profiles. This analysis was carried out for $n,m = 4$ modes and thus relatively steep gradients are necessary for destabilisation ($\omega_* \sim m$). Experimentally, energetic ICRF-generated ions easily destabilise several BAEs with different mode numbers $n = 3-6$. Simulations with realistic distribution functions are on the way.
Since BAEs tap their energy from a different region in phase space than TAEs and the overlap of resonances can couple the amplitudes of BAEs and TAEs, the saturation level of this two mode system is considerably higher that that of the single modes. This mechanism seems to explain very well the experimental loss patterns on the fast ion loss detector at ASDEX Upgrade.

The authors want to thank S.D. Pinches for his support concerning the HAGIS *code and F. Zonca for various discussions and elucidating remarks on low frequency physics.*

References

[1] G.Y. Fu, J.W. VanDam, Phys Fluids B **1**, 2404 (1989)
[2] A.D. Turnbull et al Phys. Fluids B **5**, 2546 (1993)
[3] B. Heidbrink et al, Phys. Rev. Letters **71** (1993)
[4] M. Garcia-Munoz, et al, Phys. Rev. Letters **100**, 055005 (2008)
[5] Lauber Ph. et al, J. Comp. Phys., **226/1** (2007)
[6] F. Zonca et al, Plasma Phys. Control. Fusion **38**, 2011 (1996)
[7] F. Zonca et al, Phys. Plasmas **6**, 1917 (1999)
[8] C. Nguyen et al, Phys. Plasmas **15**, 112502 (2008)
[9] A. Elfimov, Phys. Plasmas **17**, 022102 (2010)
[10] F. Zonca et al, Plasma Physics and Controlled Fusion 48, B15-B28, (2006)
[11] X. Garbet et al, Theory of Fusion Plasmas (AIP), Vol. **CP871**, p. 342 (2006)
[12] F. Zonca and L. Chen, EPL **83**, 35001 (2008)
[13] A. Smolyakov et al, Plasma Phys. Controlled Fusion **50**, 11 (2008)
[14] Z. Gao et al, Phys. Plasmas **15**, 074502 (2008)
[15] P.Villard et al, AIP Conf. Proc. **871**, 424 (2006)
[16] I. Chavdarovski and F. Zonca, Plasma Phys. Control. Fusion **51** (2009) 115001
[17] Lauber Ph. et al, Plasma Phys Control Fus., **51** (2009)
[18] F. Zonca et al, Nucl. Fusion 49 085009 (2009)
[19] Z. Guimarães Filho, private comm. (2009)
[20] V. Igochine, A. Gude, M. Maraschek and ASDEX Upgrade team: 'Hotlink based Soft X-ray Diagnostic on ASDEX Upgrade' (IPP Report 1/338); http://edoc.mpg.de/display.epl?mode=doc&id=476537
[21] P. Mc Carthy, Phys. Plasmas **6**, 3554 (1999)
[22] D. Curran et al. presented at the 37th EPS, Dublin, Ireland, (2010) EPS 2010
[23] N.N. Gorelenkov et al Phys. Lett. A **370** (2007)
[24] F. Zonca et al, Plasma Phys. Control. Fusion **48**, 537 (2006)
[25] X Wang F Zonca and L Chen, submitted to Plasma Phys. Control. Fusion
[26] F. Zonca et al, 'Kinetic Structures of shear Alfvén and acoustic wave spectra in burning plasmas', Proceedings of the Joint Varenna-Lausanne International Workshop, Varenna (2010)
[27] M. Brüdgam, PhD Thesis, TU München (2010)
[28] S.D. Pinches, Comp. Phys. Comm., **111** 133 (1998)
[29] M. Garcia-Munoz, et al, Rev. Sci Instru. **80**, (2009) 053503